ACS Sustainable Chemistry & Engineering

pubs.acs.org/journal/ascecg

Research Article

Inactivation of SARS-CoV-2 and Other Enveloped and Non-Enveloped Viruses with Non-Thermal Plasma for Hospital Disinfection

Maxime Sahun, Angela Privat-Maldonado,* Abraham Lin, Naomi De Roeck, Lisa Van der Heyden, Michaël Hillen, Johan Michiels, Gunther Steenackers, Evelien Smits, Kevin K. Ariën, Philippe G. Jorens, Peter Delputte, and Annemie Bogaerts

Cite This: *ACS Sustainable Chem. Eng.* 2023, 11, 5206−5215

Read Online

ACCESS | Metrics & More | Article Recommendations

ABSTRACT: As recently highlighted by the SARS-CoV-2 pandemic, viruses have become an increasing burden for health, global economy, and environment. The control of transmission by contact with contaminated materials represents a major challenge, particularly in hospital environments. However, the current disinfection methods in hospital settings suffer from numerous drawbacks. As a result, several medical supplies that cannot be properly disinfected are not reused, leading to severe shortages and increasing amounts of waste, thus prompting the search for alternative solutions. In this work, we report that non-thermal plasma (NTP) can effectively inactivate SARS-CoV-2 from non-porous and porous materials commonly found in healthcare facilities. We demonstrated that 5 min treatment with a dielectric barrier discharge NTP can inactivate 100% of SARS-CoV-2 (Wuhan and Omicron strains) from plastic material. Using porcine respiratory coronavirus (surrogate for SARS-CoV-2) and coxsackievirus B3 (highly resistant non-enveloped virus), we tested the NTP virucidal activity on hospital materials and obtained complete inactivation after 5 and 10 min, respectively. We hypothesize that the produced reactive species and local acidification contribute to the overall virucidal effect of NTP. Our results demonstrate the potential of dielectric barrier discharge NTPs for the rapid, efficient, and low-cost disinfection of healthcare materials.

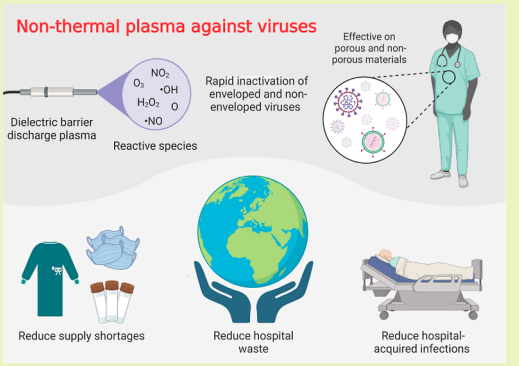

KEYWORDS: *non-thermal plasma, surface disinfection, virus inactivation, SARS-CoV-2, virucidal*

INTRODUCTION

The early 21st century has now experienced two epidemics caused by new coronaviruses, SARS-CoV-1 (2003) and MERS-CoV (2012 to present), and a pandemic caused by SARS-CoV-2 (2019 to present).[1] As reported by the World Health Organization (WHO), there have been more than 640 million confirmed cases of COVID-19 globally, including more than 6.5 million deaths to date.[2] In addition to dramatic loss of human lives worldwide, the economic and social disruption caused by the pandemic presents an unprecedented challenge to public health.[3] It has been demonstrated that SARS-CoV-2 can survive on porous materials for up to 2 days,[4] and on non-porous surfaces for up to 7 days, turning them into potential sources of infection.[5] To prevent the spread of the virus, hospitals are forced to dispose of several tons of contaminated hospital materials that could not be disinfected for safe reuse during the pandemic,[6] thus increasing the generation of waste around the world by 400−500%.[7] This led to severe shortages of medical supplies with drastic consequences for patient care.[8] As rightly pointed out by the WHO, the enormous and ever-increasing quantity of hospital waste represents a major environmental challenge, even outside of pandemic periods.[9]

The current disinfection technologies are not suitable for a broad range of materials urgently required in the hospital settings. Thermal disinfection requires long cycles (>60 min) and is not compatible with moisture- and heat-sensitive materials. Chemical disinfectants are more adapted to heat-sensitive medical items, but they are potentially toxic, flammable, or corrosive.[10] This includes low-level disinfectants that can destroy bacteria and some viruses, but not bacterial spores (e.g., sodium hypochlorite) and high-level disinfectants that can also kill bacterial spores (e.g., ethylene oxide and chlorine dioxide).[11] Furthermore, shortages of these chemicals

Received: December 24, 2022
Revised: March 10, 2023
Published: March 23, 2023

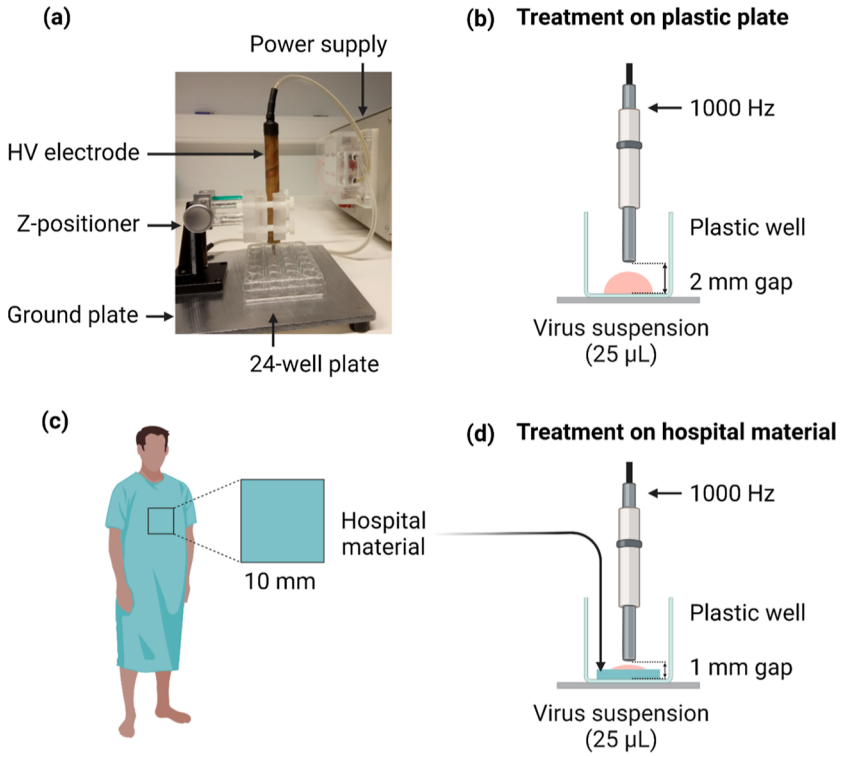

Figure 1. Experimental setup. Photograph of the DBD NTP source (a). Schematic views of the NTP treatment of viruses on plastic material (b) and on porous hospital materials (c,d).

have become an issue in times of high demand, as experienced by hospitals during the pandemic.[12] The use of ultraviolet (UV) radiation to inactivate pathogens has been an attractive alternative, but only surfaces exposed to the path of the UV light can be disinfected.[13] The environmental and economic impact of healthcare waste evidenced by the pandemic has encouraged the search for alternative easy-to-use, efficient disinfection techniques.[14]

In the past years, non-thermal plasma (NTP), a novel method that combines chemical and physical reactions,[15] has proven to be an attractive alternative for disinfection. NTP is a partially ionized gas that can be created at room temperature and atmospheric pressure. By solely using air, and without additional harmful chemicals, NTP creates highly reactive oxygen and nitrogen species (RONS; e.g., $^{\bullet}OH$, $O_2^{\bullet-}$, $^{\bullet}NO$, H_2O_2, and $ONOO^-$) which can rapidly interact with, destroy, or inactivate biological cells and pathogens.[16] It is well accepted that the rich cocktail of RONS is the main factor driving decontamination, and the UV photons and electromagnetic fields produced by NTP contribute to the generation of RONS.[17] NTP has been broadly demonstrated to inactivate bacteria and a broad range of viruses on different matrices, mainly due to its action on capsid proteins and nucleic acids.[18,19] These properties of NTP make them an attractive, environmentally friendly solution for disinfection of moisture- and temperature-sensitive supplies. Currently, there are two main categories of NTP devices for disinfection: (1) plasma jets and (2) direct dielectric barrier discharges (DBDs).[20] In plasma jets, the plasma is generated remotely with a feed gas (e.g., argon, helium, and gas mixtures) and delivered to the target via the gas flow and ionization waves.[21] On the other hand, direct DBD devices generate NTP directly onto the surface they are treating, using atmospheric air.[22] For viral disinfection, additional gas flow could further spread viral particles, and therefore, plasma jets are ill-adapted for this application. Therefore, DBD NTP devices are better adept for mitigation of contagious virus and surface disinfection.

The aim of this study is to demonstrate the potential of a DBD NTP device to inactivate SARS-CoV-2 from hospital materials, such as plastics and fabrics. For this purpose, we have characterized the inactivation of SARS-CoV-2 Wuhan and Omicron variants from plastic materials and used the porcine respiratory coronavirus (PRCV) and coxsackievirus B3 (CVB3) as safer virus models to evaluate NTP virucidal activity from porous fabrics. Our results demonstrate that NTP can effectively inactivate SARS-CoV-2 and more resistant viruses from materials commonly found in healthcare facilities. This study provides fundamental insights into the virucidal action of NTP, while supporting its value for the development as a hospital disinfection tool. Translation of this more sustainable technology would support the supply shortage, environmental impact, and healthcare consequences of future pandemics while reducing the amount of waste produced by hospitals in general.

MATERIALS AND METHODS

NTP Inactivation Experiments. *NTP Source.* NTP was generated using a microsecond-pulsed DBD plasma system (Figure 1a) previously described.[23] Briefly, the power supply was custom-built (Megaimpulse Ltd., Russia), producing a 2 μs pulse width (30 kV) with a rise time of 1−1.5 μs. The output of the power supply was connected to a DBD electrode. The DBD copper electrode (3 mm diameter) was covered with a 0.5 mm fused silica dielectric (Technical Glass). The frequency of the pulses was fixed to 1000 Hz for all experiments. The working distance, measured between the bottom of the DBD electrode and the top of the material on which the virus suspension was deposited, as well as the treatment time, were optimized for each material to obtain virus inactivation.

https://doi.org/10.1021/acssuschemeng.2c07622
ACS Sustainable Chem. Eng. 2023, 11, 5206−5215

Cell Culture and Virus Stocks. Vero (ATCC CCL-81) and swine testicular (kind gift of Prof. Nauwynck, Ghent University) cells were routinely maintained in Dulbecco's modified Eagle's medium (DMEM, Thermo Fisher Scientific) supplemented with 10% heat-inactivated fetal bovine serum (iFBS) and 2% of penicillin−streptomycin (P−S). Cells were routinely incubated at 37 °C in a CO_2 atmosphere with 95% humidity. SARS-CoV-2 Wuhan strain (lineage B Wuhan-Hu-1, 2019-nCoV-Italy-INMI1, reference 008V-03893), SARS-CoV-2 Omicron B.1.1.529.1 (BA.1) variant (strain VLD20211207: isolated and cultured at the Institute of Tropical Medicine of Antwerp),[24] human coxsackievirus B3 (ATCC VR-30), and porcine respiratory coronavirus (PRCV; strain 91V44, a kind gift of Dr. H Nauwynck, Ghent University, Belgium) were used. SARS-CoV-2 and coxsackievirus (CVB3) were grown and titrated in Vero cells. PRCV was grown and titrated in swine testicular (ST) cells. Infectious virus titers of SARS-CoV-2 and PRCV were determined by the median tissue culture infectious dose assay ($TCID_{50}$), calculated by the Reed−Muench method[25] and expressed as $\log_{10}$ $TCID_{50}$/mL. Infectious virus titer of CVB3 was determined by the plaque forming unit (PFU) assay and expressed as $\log_{10}$ PFU/mL. The titers of the virus stocks were ≈7 $\log_{10}$ $TCID_{50}$/mL for SARS-CoV-2 Wuhan strain, ≈5 $\log_{10}$ $TCID_{50}$/mL for SARS-CoV-2 Omicron variant, ≈5 $\log_{10}$ $TCID_{50}$/mL for PRCV, and ≈7 $\log_{10}$ PFU/mL for CVB3 and were directly used without dilution for NTP experiments.

NTP Treatment of Virus Suspension on Plastic Material. Viral inactivation on plastic material was done in polystyrene culture plates. A volume of 25 μL of virus suspension was deposited in the center of a well (662102 Greiner Bio-One CELLSTAR cell culture plate, 24-well, flat bottom) and immediately treated with the DBD with a frequency of 1000 Hz, and an optimal working distance of 2 mm (Figure 1b). NTP treatments were carried out for 5 min for SARS-CoV-2 and PRCV and 10 min for CVB3. Immediately after the NTP treatment, 100 μL of DMEM (2% iFBS, 2% P−S) was added to rinse the well and to allow for virus recovery. The total volume was collected and used for titration. The evaporation due to NTP treatment was taken into account to obtain corrected values of infectious titer per volume. A non-treated virus suspension (25 μL) was processed similarly and used as a negative control. All measurements were performed with at least three biological replicates and three independent replicates.

NTP Treatment of Virus Suspension on Porous Hospital Materials. Hospital pillowcase (fabric 1) and hospital gown (fabric 2) were selected as representative porous hospital materials. Fabric 1 was made of 100% cotton fibers and fabric 2 was made of a blend of cotton and synthetic polyester. Hospital fabrics were cut in 1 cm^2 pieces and immersed in 90% ethanol solution for cleaning. The samples were rinsed in Milli-Q water and allowed to dry overnight in a safety cabinet. The sample were positioned in the center of a well (662102 Greiner Bio-One CELLSTAR cell culture plate, 24-well, flat bottom) and 25 μL of virus suspension was deposited at the surface of the sample. After 30 min of incubation, the sample was treated with the DBD with a frequency of 1000 Hz, an optimal working distance of 1 mm and during 5 min for PRCV and 10 min for CVB3 (Figure 1c). Immediately after the NTP treatment, 200 μL of DMEM (2% iFBS, 2% P−S) was added in the well to cover the sample and the plate was placed in an orbital shaker (150 RPM) for 30 min for virus recovery. In comparison with the treatment on the plastic plate, the volume to rinse the well was increased (from 100 to 200 μL) to ensure a full immersion of the sample in the liquid. The total volume in the well was collected and used for titration. A non-treated virus suspension (25 μL) was processed similarly and used as a negative control. All measurements were performed with at least three biological replicates and three independent replicates.

$TCID_{50}$ Titration of SARS-CoV-2 and PRCV. The titer of both strains of SARS-CoV-2 was assessed following the $TCID_{50}$ method in Vero cells in a 96-well format. Each recovered sample was subjected to 10-fold serial dilutions and incubated in 4-fold with freshly plated 1.8×10^4 Vero cells for 1 week (37 °C, 5% CO_2). After 7 days, the wells were examined microscopically for the presence of the viral cytopathic effect caused by viral growth, and the virus titer was calculated using the Reed−Muench method.

The titer of PRCV samples was assessed following the $TCID_{50}$ method in ST cells in a 96-well format. Each recovered sample was subjected to 10-fold serial dilutions and incubated in 6-fold with 1 day old plated 2×10^4 ST cells in 96-well plates for 1 week (37 °C, 5% CO_2). After 6 days, the presence of the viral cytopathic effect was microscopically evaluated and the virus titer was calculated using the Reed−Muench method. The detection limits are 2.4 $\log_{10}$ $TCID_{50}$/mL for SARS-CoV-2 and 1.3 $\log_{10}$ $TCID_{50}$/mL for PRCV.

CVB3 Plaque Assay. The titer of CVB3 samples was assessed in Vero cells in a 6-well format. Each recovered sample was subjected to 10-fold serial dilutions and incubated in 4-fold with 1 day old plated 1.3×10^6 Vero cells for 1 h (37 °C, 5% CO_2) with agitation every 15 min. The viral medium was aspirated and the infected cell layer was covered by a 0.6% Avicel solution with DMEM (10% iFBS, 2% P−S, 3 mL/well) and incubated for 2 days (37 °C, 5% CO_2). Avicel overlay was removed and the cells were fixed with 4% paraformaldehyde solution and stained with 0.25% crystal violet. The number of visible plaques caused by viral growth was determined and used for PFU titer calculation. The detection limit was 1.9 $\log_{10}$ PFU/mL.

Thermal Imaging. Thermal images were recorded using a cooled FLIR x6540sc thermal imaging camera during NTP treatment of 25 μL of DMEM (2% iFBS, 2% P−S) in a 24-well plate. The camera has an InSb detector with a resolution of 640 × 512 pixels, with a measurement accuracy of ±1 °C, and a thermal sensitivity/noise equivalent temperature difference < 25 mK. Measurements were carried out without filter and using an L1206 50 mm $f = 3$ lens, which has a spectral range of 1.5−5 μm. All NTP discharges were observed with a frame rate of 30 fps and the image sequences were recorded using FLIR Researcher IR Max software. Afterward, all data were processed in MathWorks MATLAB. The data were obtained and processed at the Industrial Vision Lab (InViLab), University of Antwerp.

pH Measurement. The DBD was used to treat 25 μL DMEM (2% iFBS, 2% P−S) in a 24-well plate. The working distance was 2 mm and NTP was generated at a 1000 Hz pulse frequency and varying treatment times. The remaining volume was collected in Eppendorf tubes directly after the treatment and the pH was analyzed in 30 min following the treatment with a custom-made pH microprobe ("Leak Free" 1 mm pH probe AMANI 1000L, Harvard Apparatus) from the Applied Electrochemistry & Catalysis (ELCAT) research group from the University of Antwerp, in a minimum volume of 10 μL. All measurements were performed at least three times on three independent replicates.

RONS Quantification. The DBD NTP system was used to treat 25 μL DMEM (2% iFBS, 2% P−S) in a 24-well plate. The working distance was 2 mm and NTP was generated at a 1000 Hz pulse frequency and varying treatment times. Following the treatment, 1 mL of (2% iFBS, 2% P−S) was immediately added to rinse the well. The total volume was collected and analyzed. The evaporation of treated medium due to NTP treatment was measured for each treatment time and taken into account to obtain the corrected values of RONS concentration. All chemical measurements were performed at least three times on three independent replicates.

For the quantification of NO_3^- and NO_2^-, a fluorometric assay kit (780051; Cayman Chemical) was used according to the manufacturer's instructions. To measure both NO_3^- and NO_2^- (NO_3^- + NO_2^-), 20 μL of 20× diluted samples was added in a 96-well plate and the volume was adjusted to 80 μL using DMEM (2% iFBS, 2% P−S). A nitrate reductase mixture (780010; Cayman Chemical) and an enzyme cofactor mixture (780012; Cayman Chemical) were added to each well and incubated for 1 h, allowing for the conversion of NO_3^- into NO_2^-. DAN reagent (780070; Cayman Chemical) provided as an acidic solution was added to each well and incubated for 10 min before adding NaOH (780068; Cayman Chemical), which enhances the detection of the fluorescent product 1(H)-naphtotriazole. The plate was read with the Tecan Spark Cyto (λ_{ex}: 365 ± 20 nm, λ_{em}: 430 ± 20 nm, fixed gain: 64). To measure NO_2^-, 20 μL of 10× diluted samples was added in a 96-well plate and the volume was

https://doi.org/10.1021/acssuschemeng.2c07622
ACS Sustainable Chem. Eng. 2023, 11, 5206−5215

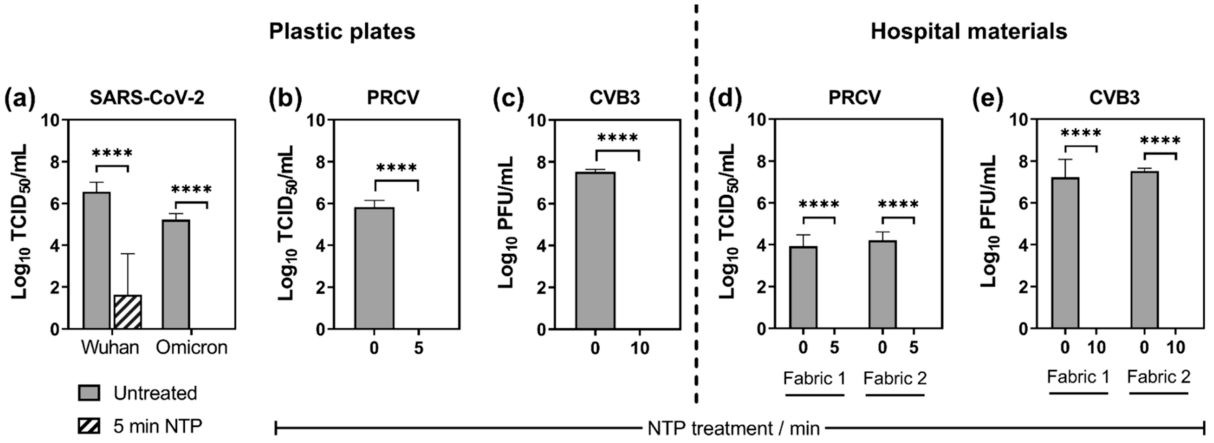

Figure 2. NTP inactivation of viruses on plastic plates (left) and hospital materials (right). Mean values of infectious titers before and after NTP treatment on plastic plates for SARS-CoV-2 Wuhan strain and Omicron variant (a), PRCV (b), and CVB3 (c). Mean values of infectious titers before and after treatment on hospital materials for PRCV (d) and CVB3 (e). Error bars indicate standard deviation (n = 3). ND: not detected (detection limits: 2.4 $\log_{10}$ $TCID_{50}$/mL for SARS-CoV-2, 1.9 $\log_{10}$ PFU/mL for CVB3, and 1.3 $\log_{10}$ $TCID_{50}$/mL for PRCV). **** p-value < 0.0001 by Student's t-test.

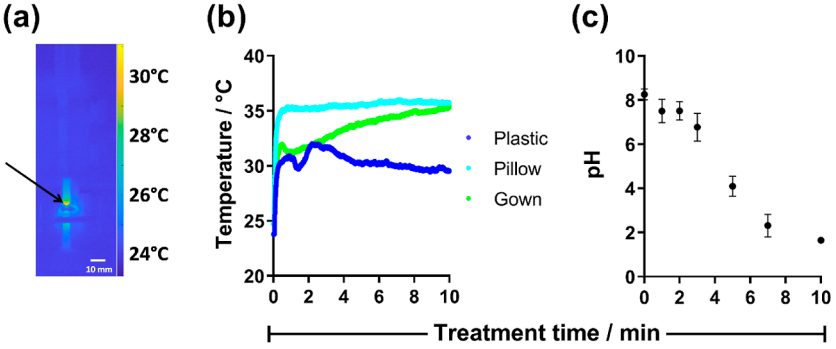

Figure 3. Physical characterizations of NTP treatment. Thermal imaging (a) and measurement of local temperature (b) at the tip of the DBD electrode (black arrow) for different treatment times. Measurement of pH value (c). Mean ± S.D. (n = 3).

adjusted to 100 μL using DMEM (2% iFBS, 2% P−S). DAN reagent (780070; Cayman Chemical) was directly added to each well and incubated for 10 min before adding NaOH (780068; Cayman Chemical) and reading the plate with Tecan Spark Cyto (λ_{ex}: 365 ± 20 nm, λ_{em}: 430 ± 20 nm, fixed gain: 81). An estimate of NO_3^- concentrations was, therefore, calculated by subtracting the mean NO_2^- concentration of each treatment condition from the NO_3^- + NO_2^- concentration. Concentrations of NO_3^- and NO_2^- were calculated from a calibration curve, obtained using standard solutions provided in the assay kit.

For the quantification of H_2O_2, a fluorometric assay kit (MAK165; Merck) was used according to the manufacturer's instructions. A volume of 50 μL of 10× diluted samples (in DMEM 2% iFBS, 2% P−S) was added in a 96-well plate and mixed with 50 μL of a master mix containing 4.75 mL of assay buffer + 50 μL of red peroxidase substrate + 200 μL (20 units/mL) peroxidase. The samples were incubated for 30 min and the fluorescence was measured using the Tecan Spark Cyto (λ_{ex}: 540 ± 20 nm, λ_{em}: 590 ± 20 nm, fixed gain: 54). Concentrations of H_2O_2 were calculated from a calibration curve, obtained using standard solution provided in the assay kit.

Statistical Analysis. Student's t-test was performed using Prism v9.3.1 (GraphPad Software, San Diego, CA, USA). Statistical significance was set at $p \leq 0.05$.

RESULTS

SARS-CoV-2 Inactivation on Plastic Material. Two strains of SARS-CoV-2 were treated with NTP on plastic plates. For the SARS-CoV-2 Wuhan strain, 5 min of NTP treatment reduced the initial infectious titer by 4.9 $\log_{10}$ (6.5−1.6 $\log_{10}$ $TCID_{50}$/mL; Figure 2a). This reduction was equivalent to a complete inactivation since on average, the obtained infectious titer after treatment (1.6 $\log_{10}$ $TCID_{50}$/mL) was below the detection limit of the titration method (2.4 $\log_{10}$ $TCID_{50}$/mL). For the SARS-CoV-2 BA.1 Omicron variant, NTP completely inactivated the viral sample after 5 min of treatment (Figure 2a). These results demonstrate that NTP can effectively inactivate SARS-CoV-2 from plastic material.

Virus Models' Inactivation on Porous Hospital Materials. Once NTP was demonstrated to inactivate both the Wuhan and Omicron strains of SARS-CoV-2, PRCV and CVB3 were used as virus models to investigate NTP disinfection of porous hospital materials, as these viruses could be more easily handled in BSL-2 facilities. The response of the virus models to NTP was preliminarily assessed on a plastic plate in the same way as for SARS-CoV-2. NTP completely inactivated PRCV after 5 min of treatment (with ≥5.8 $\log_{10}$ TCID50/mL reduction; Figure 2b) and CVB3 after 10 min of treatment (with ≥7.5 $\log_{10}$ PFU/mL reduction; Figure 2c). Altogether, these data demonstrate that NTP was able to rapidly inactive both the SARS-CoV-2 virus strains as well as PRCV and non-enveloped CVB3.

We then assessed viral inactivation from porous hospital materials using fabrics from hospital bed pillowcases (fabric 1)

https://doi.org/10.1021/acssuschemeng.2c07622
ACS Sustainable Chem. Eng. 2023, 11, 5206−5215

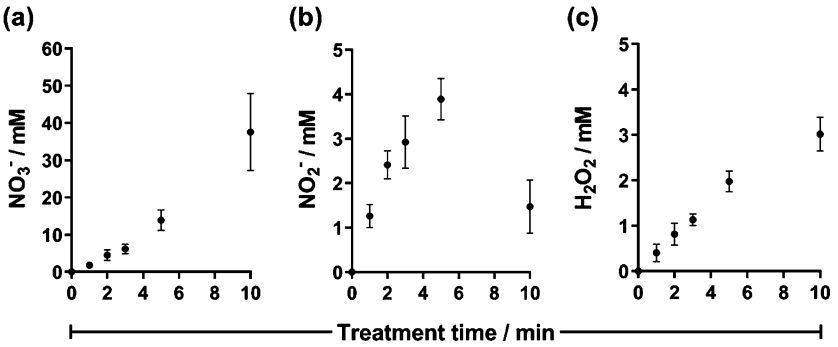

Figure 4. Chemical characterization of NTP treatment. NO_3^- (a), NO_2^- (b) ions, and H_2O_2 (c) concentrations in liquid medium for different treatment times. Mean ± S.D. (n = 3).

and hospital gowns (fabric 2), artificially contaminated with PRCV and CVB3. For PRCV, NTP completely reduced the initial infectious titer after 5 min of treatment for both fabrics (fabric 1: ≥3.9 $\log_{10}$ $TCID_{50}$/ml reduction; fabric 2: ≥4.2 $\log_{10}$ $TCID_{50}$/ml reduction; Figure 2d). For CVB3, NTP achieved complete reduction of the initial infectious titer after 10 min of treatment (fabric 1: ≥7.2 $\log_{10}$ PFU/mL; fabric 2: ≥7.5 $\log_{10}$ PFU/mL; Figure 2e).

Our results demonstrate that NTP can inactivate PRCV using the same conditions as for SARS-CoV-2, possibly due to the direct effect of RONS on the lipid envelope, which affects the viral infectivity. Thus, PRCV is a suitable surrogate virus to assess SARS-CoV-2 viral disinfection with NTP. On the other hand, CVB3 appeared to be more resistant to NTP. The inactivation of non-enveloped viruses such as CVB3 requires the denaturation of the capsid proteins and damage to the RNA,[10] which makes them more resistant to disinfection, as shown here.

Effect of Temperature and pH on NTP Viral Inactivation. To investigate the underlying mechanisms of NTP-based viral inactivation, we measured the evolution of the local temperature at the tip of the DBD electrode (Figure 3a, white arrow) continuously during NTP treatment of the different samples (plastic, fabrics 1, and fabric 2; Figure 3b). During the first 30 s following NTP initiation, the temperature was increased by 6 to 10 °C for the different samples, with the local temperature never exceeding 35 °C, even after 10 min of treatment. Therefore, it was clear that NTP treatment temperature was not responsible for its virucidal effects.

As low pH is also known to denature viruses[26] and NTP has acidification effects,[27] we assessed the pH of NTP-treated medium at the equivalent treatment times and conditions used for viral inactivation. Our results demonstrate that the pH decreased over the course of treatment (Fig. 3-c), reaching pH = 4 after 5 min of treatment and pH = 1.6 after 10 min. Therefore, it is possible that the acidification of the liquid solution contributes to the mechanism of viral inactivation by NTP treatment.

NO_3^-, NO_2^-, and H_2O_2 Quantification. To determine the role of the reactive species present in the NTP-treated solutions, we assessed the concentrations of NO_3^-, NO_2^-, and H_2O_2 in NTP-treated medium (without virus) at different treatment times. The concentrations of NO_3^- and H_2O_2 were time-dependent, with longer exposure times leading to higher concentrations (Figure 4a,c). After exposure to NTP, NO_3^- and H_2O_2 were measured to be 14 ± 2.78 and 2 ± 0.23 mM, respectively, at 5 min and 38 ± 10.4 and 3 ± 0.38 mM, respectively, at 10 min. Interestingly, NO_2^- concentrations demonstrated a similar behavior up to 5 min (4 ± 0.47 mM), before dropping for 10 min of treatment (1.5 ± 0.60 mM; Figure 4b). We speculate that the antiviral activity of NTP is partially mediated by the effect of the reactive species measured here. However, we acknowledge that other relevant NTP-induced reactive species could be present in the treated medium such as peroxynitrite ($ONOO^-$),[28] but were not measured in this study.

DISCUSSION

The recent SARS-CoV-2 pandemic has highlighted the need for new technologies to disinfect clinical settings and materials. Not only is this required for proper care of patients and healthcare workers, but it is also needed to reduce supply shortages, healthcare costs, and waste production. In this study, we used NTP technology to inactivate SARS-CoV-2 (the most relevant Wuhan and Omicron strains), PRCV, and CVB3 from porous and non-porous hospital materials. We demonstrated that the DBD is able to completely inactivate SARS-CoV-2 and surrogate viruses after only 5−10 min of treatment. Compared to hospital room surfaces, which have been reported to have the presence of 0.1 to 102 SARS-CoV-2 RNA genome copies per square centimeter (gc/cm^2),[29] the viral loads used in our work were significantly higher: 500,000 times higher for the Wuhan strain and 1000 times higher for the Omicron variant.[29,30] This further demonstrates the ability of NTP technology to rapidly and effectively inactivate high viral loads from various hospital materials (log 5 reduction) and complies with the requirements of the European Union standards for virus-inactivating disinfectants (reduction > log 4).[31] Our results also provide insights into the efficacy of NTP against viruses and highlight the potential of NTP for surface decontamination.

In the present work, we used enveloped (SARS-CoV-2 and PRCV) and non-enveloped (CVB3) viruses to test the antiviral activity of our DBD plasma system. Both SARS-CoV-2 and PRCV are enveloped RNA viruses that belong to the *Coronaviridae* family and present morphological, biophysical, and genomic similarities,[32] which makes PRCV a suitable surrogate virus model for SARS-CoV-2. The parameters required for NTP inactivation of SARS-CoV-2 and the surrogate virus PRCV were similar, while longer treatment times were needed for the CVB3 virus. CVB3, a human non-enveloped RNA enterovirus, is more resistant to common disinfection methods[33] and to environmental stressors, such as desiccation and temperature changes, compared to that of enveloped viruses.[34] Viral inactivation of both virus types via

https://doi.org/10.1021/acssuschemeng.2c07622
ACS Sustainable Chem. Eng. 2023, 11, 5206−5215

RONS is mediated by oxidative damage to proteins, viral envelopes (when present), and nucleic acids.[19] For example, it has been demonstrated that NTP-derived RONS damage the receptor-binding domain of the spike (S) protein of SARS-CoV-2, key for its anchorage to host cells, thus reducing its ability to infect cells.[35] These RONS can also degrade the viral RNA from aerosols and surfaces.[36,37] NTP produces a wide variety of RONS with antiviral properties, such as singlet oxygen ($^1O_2$), hydroxyl radical ($^{\bullet}OH$), superoxide ($O_2^{\bullet-}$)/hydroperoxyl radicals (HO_2), H_2O_2, ozone (O_3), nitric oxide ($^{\bullet}NO$), $ONOO^-$, NO_3^-, NO_2^-, and nitrous acid (HNO_2).[38] We have demonstrated in our previous work that many of these RONS are produced by our DBD, including $ONOO^-$.[28] $ONOO^-$ can be generated directly from HNO_2 and H_2O_2 under acidic conditions and plays a central role in viral inactivation.[39,40] It is then quite likely that $ONOO^-$ is also formed in the NTP-treaded solutions shown here and participates in the inactivation process, yet this needs to be further studied. Some NTP studies have described NTP-derived O_3 as the main RONS responsible for viral inactivation of porous/non-porous materials and aerosols.[37,41,42] However, the levels of O_3 produced by such devices (800 ppm) highly exceed the permissible exposure limit of 0.1 ppm and do not consider a processing unit to reduce the O_3 levels after treatment, while other NTPs can produce significantly lower amounts of O_3.[43,44] This is an issue that must be addressed before these NTP sources become available for commercial use. In our study, we found that NTP produced high levels of H_2O_2 and NO_3^- in the liquid. H_2O_2 is known to effectively inactivate viruses and bacteria,[45] but NO_3^- alone does not have the same effect.[38] However, in our NTP treatment setup, it is unlikely that H_2O_2 is the main cause of viral inactivation, as the concentrations (approx. 3 mM in 10 min) are too low (Figure 4c). In fact, a study by Bidra et al., investigated the efficacy of H_2O_2 for SARS-CoV-2.[46] In that report, the authors demonstrated that H_2O_2 solutions at clinically recommended and commercially available concentrations of 3.0% w/w (88.2 mM) and 1.5% w/w (44.1 mM) had minimal viricidal activity against SARS-CoV-2. Another study also demonstrated that 3.0% w/w H_2O_2 at a pH of 7.3 could not inactivate SARS-CoV-2, even with a contact time of up to 15 min.[47] Interestingly, when the pH was lowered to 2.5 with citric acid, there was some inactivation at 5 min, but it was not complete. This combination of H_2O_2 and acidification could participate in the mechanism of NTP-viral inactivation, though here, we saw complete inactivation of the SARS-CoV-2 Omicron variant within 5 min of treatment (Figure 2a). Therefore, it is likely that, as with other biomedical applications[48] the short-lived reactive species, such as $^{\bullet}OH$ and $O_2^{\bullet-}$, are also involved in the NTP mechanism of action. Indeed, we have previously demonstrated both in silico and in vitro that the short- and long-lived species produced by NTP oxidize proteins, lipids, nucleic acids, and glycosaminoglycans present in eukaryotic and prokaryotic cells.[23,49−51] These biomolecules are the essential building blocks of the viral particles and are susceptible to oxidative damage by NTP. Thus, the inactivation of SARS-CoV-2 by NTP could be the result of oxidative damage to multiple components simultaneously. The concentrations of RONS produced by NTP are low compared to other disinfection approaches based on H_2O_2,[46] yet they are sufficient to decrease the infectivity of SARS-CoV-2.

The viral inactivation observed here is also unlikely to be due to the effect of UV radiation. A previous study done with a similar NTP source showed that the DBD produces approx. 4.5 mJ/cm^2 UV radiation in 5 min (retrospectively calculated from ref 22). However, low-pressure UV lamps require from 1.3 to 60 mJ/cm^2 to achieve 90% inactivation of SARS-CoV-2 in aqueous solutions (1-log reduction).[52,53] In our work, we obtained the complete inactivation of SARS-CoV-2 after 5 min of DBD NTP treatment (4.9-log reduction). In addition, it has been observed that removing the RONS and allowing only the pass of UV radiation completely removes the ability of NTP to inactivate pathogens.[54] Based on our current and previous results,[48] we hypothesize that the unique combination of RONS produced by the DBD makes the treatment effective due to the simultaneous multitarget activity of NTP-derived RONS.[55]

Regarding the role of temperature in viral inactivation, it is known that coronaviruses and coxsackieviruses require temperatures of around 50 °C to reduce their infectivity.[56,57] Therefore, the virucidal activity of our NTP source was not due to thermal damage, as in all cases, the temperature remained below 35 °C. However, the low pH of the solutions could play a role in the inactivation process. The pH reduction observed in NTP-treated solutions has been consistently reported in the literature[58−60] and has been explained by the formation of HNO_2 and nitric acid (HNO_3) via reactive nitrogen species, like $^{\bullet}NO$ and nitrogen oxides, initially generated in atmospheric pressure humid air NTP. Another hypothesis is the generation of acidic H_3O^+ ions by reactions of water with H_2O_2 generated in air or liquid medium.[27] Previous studies have shown that SARS-CoV-2 remains viable on solutions at pH = 4 to 11 for several days, and CVB3 can remain viable for 7 days at pH = 2.3 to 9.[61,62] However, it has been suggested that the stability of viral proteins required for cell infection is significantly reduced at pH values below 6.[63] Thus, it is possible that the antiviral activity of NTP observed is enhanced by the acidic conditions,[58,64−66] increasing the oxidation efficiency and the susceptibility of viruses against low pH.[27]

Our results demonstrate the ability of NTP to inactivate different viruses from porous and non-porous materials, in agreement with the literature.[18,67,68] The different levels of roughness and absorptivity of the materials must be considered when determining the treatment times for complete viral inactivation of plastics, metals, and cardboard, for example.[69] Some of the most common materials in the healthcare industry are cotton and cotton-blend textiles (such as gowns and face masks),[70] which can retain moist and viral particles due to their porosity. Although fabrics can be disinfected with hot water, detergents, or disinfectants,[71] these methods are not suitable for every textile (i.e., cotton-based protective personal equipment; PPE). For non-porous materials, classic disinfectants based on oxidizing agents, such as sodium hypochlorite, hydrogen peroxide, and peracetic acid, are fast-acting and efficient against a broad range of viruses, but are often limited by their toxicity and damaging effects to treated surfaces.[10] Our study indicates that NTP can be an environmentally friendly alternative, for both porous and non-porous materials.

Indeed, the COVID-19 pandemic evidenced the need to decontaminate multiple types of materials for safe reuse and to reduce the financial burden and waste production by the healthcare sector, as suggested by the WHO.[72] Even during non-pandemic periods, hospitals produce more than 1.2

https://doi.org/10.1021/acssuschemeng.2c07622
ACS Sustainable Chem. Eng. 2023, 11, 5206−5215

million tons of plastic waste per year from both used and unused medical supplies that cannot be reused or recovered.[72] This represents an environmental and financial challenge for the healthcare systems. The amount of medical waste and the associated costs are remarkable and highlights the need for better disinfection tools suitable for a broad range of materials.[73] In this context, DBD NTP technology could be a suitable tool to disinfect hospital supplies. In addition, solutions like DBD NTPs could be part of the prevention strategies to strengthen the global preparedness against future public-health crises.

The WHO guidelines for disinfection provide a list of conditions that an ideal disinfectant must: (1) have a high germicidal activity against a wide range of microorganisms, (2) be chemically stable, (3) be effective in the presence of organic compounds, (4) be compatible with the surface being disinfected, (5) be able to penetrate into crevices (desirable), and (6) be inexpensive and aesthetically acceptable.[74] NTP satisfies these proposed conditions, compared to many current state-of-the-art devices and methods. The rapid and complete inactivation obtained for the viruses on porous and non-porous materials reveals the high efficiency of DBD NTP in inactivating not only SARS-CoV-2 but also highly resistant human viruses from hospital materials. The advantage of the DBD NTP source is that it does not require the addition of chemicals or components, as it uses atmospheric air, thus making it operationally inexpensive. In addition, the low temperatures and short treatment times further make DBD NTP an attractive technology for decontamination. In DBD NTP sources, only the electricity costs for powering the device have to be accounted for, but NTP is ideally suited to be combined with renewable electricity due to its short switch on/off times.[75] Other studies have reported viral inactivation with different NTP devices but not without drawbacks.[76] The need of vacuum systems,[15] feed gases,[69,77−79] high gas temperatures that can damage the materials,[80,81] or very long treatment times[82] make those devices unsuitable for routine hospital use. Moreover, gas-fed NTP, such as plasma jets, could present additional health risks, as the constant gas flow could blow microdroplets that carry viruses and other contaminating particles into the surrounding environment, thus further spreading its reach. Another strategy which uses NTP for disinfection is via generation of NTP-treated liquids, such as water.[83,84] In this modality, NTP is used to treat and enrich a liquid with RONS. This liquid is then applied to the surface to be disinfected. However, a major drawback is that it can only be used on wettable surfaces. This drawback is similar to the use of super-oxidized water, where an electrical current is passed through salt water to generate species such as hypochlorous acid, dissolved oxygen, superoxide radicals, and more.[85] Furthermore, the time between NTP liquid treatment and liquid application to the surface is critical, as several RONS, particularly the short-lived RONS, are unstable over time. Interestingly, Guo et al., has reported that $^1O_2$, a short-lived RONS, could have an important function in bacteriophage inactivation with NTP-treated water, thus further highlighting the importance of RONS stability in NTP-treated liquids.[84] If there is a significant delay between NTP enrichment of the liquid and application to the surface for disinfection, then the NTP-treated liquid is nothing more than a combination of the stable RONS (e.g., H_2O_2, NO_2^-, and NO_3^-), which can easily be made through commercial products.

DBD NTP technology does not have the drawbacks of plasma jets and NTP-treated liquids and therefore is most ideal for inactivation of contagious viruses, such as SARS-CoV-2, from medical products that cannot be decontaminated otherwise in a safe manner. Direct generation of DBD onto the surface for disinfection guarantees the delivery of the potent, short-lived RONS (e.g., singlet oxygen, atomic oxygen, and hydroxyl radicals). We believe that large-scale DBD NTP devices for disinfection of hospital materials are novel, sustainable solutions to help reduce costs and waste production, for both future pandemics as well as routine daily practice. However, there are several parameters that must be optimized, such as NTP treatment time. This is partially dependent on the material being disinfected, as there requires a balance between adequate viral inactivation and preventing damage to treated materials. Research into new geometric designs and scalability is needed and is currently ongoing in our lab.

CONCLUSIONS

In this work, we successfully used NTP technology to inactivate SARS-CoV-2, PRCV, and CVB3 from porous and non-porous materials commonly found in hospitals. DBD NTP is an attractive, environmentally friendly solution for disinfection of moisture- and temperature-sensitive materials without the need of additional gases or chemicals and should be further explored. This is a proof-of-concept study, and the device can be scaled up for large capacity disinfection. This technology has the potential to prevent hospital-acquired infections, supply shortages, and reduce the waste produced by healthcare facilities. We envision that NTP devices based on this concept could also be adopted into other market sectors, such as ambulatory medicine, elderly homes, hospitality, and schools.

AUTHOR INFORMATION

Corresponding Author

Angela Privat-Maldonado − *Plasma Lab for Applications in Sustainability and Medicine—Antwerp (PLASMANT), Department of Chemistry, University of Antwerp, 2610 Antwerp, Belgium; Center for Oncological Research (CORE), Integrated Personalized & Precision Oncology Network (IPPON), University of Antwerp, 2610 Antwerp, Belgium;* orcid.org/0000-0002-5616-8182; Email: angela.privatmaldonado@uantwerpen.be

Authors

Maxime Sahun − *Plasma Lab for Applications in Sustainability and Medicine—Antwerp (PLASMANT), Department of Chemistry, University of Antwerp, 2610 Antwerp, Belgium*

Abraham Lin − *Plasma Lab for Applications in Sustainability and Medicine—Antwerp (PLASMANT), Department of Chemistry, University of Antwerp, 2610 Antwerp, Belgium; Center for Oncological Research (CORE), Integrated Personalized & Precision Oncology Network (IPPON), University of Antwerp, 2610 Antwerp, Belgium;* orcid.org/0000-0003-0097-3323

Naomi De Roeck − *Laboratory for Microbiology, Parasitology and Hygiene (LMPH), Faculty of Pharmaceutical, Biomedical and Veterinary Sciences, University of Antwerp, 2610 Antwerp, Belgium*

https://doi.org/10.1021/acssuschemeng.2c07622
ACS Sustainable Chem. Eng. 2023, 11, 5206−5215

Lisa Van der Heyden − *Plasma Lab for Applications in Sustainability and Medicine—Antwerp (PLASMANT), Department of Chemistry, University of Antwerp, 2610 Antwerp, Belgium; Center for Oncological Research (CORE), Integrated Personalized & Precision Oncology Network (IPPON), University of Antwerp, 2610 Antwerp, Belgium*

Michaël Hillen − *Industrial Vision Lab (InViLab), Department of Electromechanical Engineering, University of Antwerp, 2020 Antwerp, Belgium;* orcid.org/0000-0001-5859-8402

Johan Michiels − *Virology Unit, Department of Biomedical Sciences, Institute of Tropical Medicine Antwerp, 2000 Antwerp, Belgium*

Gunther Steenackers − *Industrial Vision Lab (InViLab), Department of Electromechanical Engineering, University of Antwerp, 2020 Antwerp, Belgium*

Evelien Smits − *Center for Oncological Research (CORE), Integrated Personalized & Precision Oncology Network (IPPON), University of Antwerp, 2610 Antwerp, Belgium*

Kevin K. Ariën − *Laboratory for Microbiology, Parasitology and Hygiene (LMPH), Faculty of Pharmaceutical, Biomedical and Veterinary Sciences, University of Antwerp, 2610 Antwerp, Belgium; Virology Unit, Department of Biomedical Sciences, Institute of Tropical Medicine Antwerp, 2000 Antwerp, Belgium*

Philippe G. Jorens − *Department of Intensive Care Medicine, Antwerp University Hospital, 2650 Antwerp, Belgium; Laboratory of Experimental Medicine and Pediatrics (LEMP), University of Antwerp, 2610 Antwerp, Belgium*

Peter Delputte − *Laboratory for Microbiology, Parasitology and Hygiene (LMPH), Faculty of Pharmaceutical, Biomedical and Veterinary Sciences, University of Antwerp, 2610 Antwerp, Belgium*

Annemie Bogaerts − *Plasma Lab for Applications in Sustainability and Medicine—Antwerp (PLASMANT), Department of Chemistry, University of Antwerp, 2610 Antwerp, Belgium;* orcid.org/0000-0001-9875-6460

Complete contact information is available at: https://pubs.acs.org/10.1021/acssuschemeng.2c07622

Author Contributions

M.S.: conceptualization, methodology, validation, formal analysis, investigation, and writing—original draft. A.P.-M.: conceptualization, writing—original draft, and writing—reviewing and editing. A.L.: conceptualization and writing—reviewing and editing. N.D.R.: methodology. L.V.d.H.: investigation and validation. M.H.: investigation. J.M.: investigation. G.S.: resources. E.S.: resources and supervision. K.K.A.: resources. P.G.J.: conceptualization and resources. P.D.: resources and supervision. A.B.: resources, supervision, and funding acquisition.

Notes

The authors declare no competing financial interest.

[▽]M.S. and A.P.-M. share the first authorship.

■ ACKNOWLEDGMENTS

This work was supported by the Research Foundation—Flanders (FWO), i.e., FWO fellowships and grants 12S9221N (Abraham Lin), G033020N (Annemie Bogaerts), G0G4220N (Kevin K. Ariën), and G044420N (Abraham Lin, Annemie Bogaerts, and Steve Vanlanduit), and the University of Antwerp Industrial Research Fund (IOF-POC project). Michaël Hillen was supported by the University of Antwerp grant BOF DOCPRO ID 39928. LMPH is partner of the "Infla-Med" Centre of Excellence. The authors thank the Research Group on Applied Electrochemistry & Catalysis (ELCAT) from the University of Antwerp for providing the pH meter. Graphical abstract and Figure [1] created with Biorender.com.

■ REFERENCES

(1) Edwards, A. M.; Baric, R. S.; Saphire, E. O.; Ulmer, J. B. Stopping Pandemics before They Start: Lessons Learned from SARS-CoV-2. *Science* **2022**, *375*, 1133−1139.

(2) WHO. WHO Coronavirus (COVID-19) Dashboard. https://covid19.who.int (accessed May 18, 2022).

(3) United Nations. Department of Economic and Social Affairs Social Inclusion. Everyone Included: Social Impact of COVID-19| DISD. https://www.un.org/development/desa/dspd/everyone-included-covid-19.html (accessed May 18, 2022).

(4) Owen, L.; Shivkumar, M.; Laird, K. The Stability of Model Human Coronaviruses on Textiles in the Environment and during Health Care Laundering. *Msphere* **2021**, *6*, e00316−e00321.

(5) Jabłońska-Trypuć, A.; Makuła, M.; Włodarczyk-Makuła, M.; Wołejko, E.; Wydro, U.; Serra-Majem, L.; Wiater, J. Inanimate Surfaces as a Source of Hospital Infections Caused by Fungi, Bacteria and Viruses with Particular Emphasis on SARS-CoV-2. *Int. J. Environ. Res. Public Health* **2022**, *19*, 8121.

(6) Tang, K. H. D. Medical Waste during COVID-19 Pandemic: Its Types, Abundance, Impacts and Implications. *Ind. Domest. Waste Manag.* **2022**, *2*, 71−83.

(7) United; Nations Environment Programme, International Environmental Technology Centre (IETC), IGES. Waste Management during the COVID-19 Pandemic: from response to recovery. http://www.unep.org/resources/report/waste-management-during-covid-19-pandemic-response-recovery (accessed Oct 21, 2022).

(8) Grand View Research. Global Medical Textiles Market Size Report, 2021-2028. https://www.grandviewresearch.com/industry-analysis/medical-textiles-market (accessed Oct 20, 2022).

(9) WHO. Health-care waste. https://www.who.int/news-room/fact-sheets/detail/health-care-waste (accessed Dec 7, 2022).

(10) Lin, Q.; Lim, J. Y. C.; Xue, K.; Yew, P. Y. M.; Owh, C.; Chee, P. L.; Loh, X. J. Sanitizing Agents for Virus Inactivation and Disinfection. *View* **2020**, *1*, No. e16.

(11) Wilson, A. J.; Nayak, S. S. Disinfection, sterilization and disposables. *Anaesth. Intensive Care Med.* **2019**, *20*, 603−608.

(12) Leonardi Vinci, D. L.; Polidori, P.; Miljković, N.; Batista, A.; Amann, S.; Makridaki, D.; Kohl, S. Lessons Learnt from the COVID-19 Pandemic: Results of EAHP Survey on the Future Crisis Preparedness of Hospital Pharmacies. *Eur. J. Hosp. Pharm.* **2021**, *29*, 242.

(13) Andersen, B. M.; Bånrud, H.; Bøe, E.; Bjordal, O.; Drangsholt, F. Comparison of UV C Light and Chemicals for Disinfection of Surfaces in Hospital Isolation Units. *Infect. Control Hosp. Epidemiol.* **2006**, *27*, 729−734.

(14) Klemeš, J. J.; Fan, Y.; Jiang, P. The Energy and Environmental Footprints of COVID-19 Fighting Measures−PPE, Disinfection, Supply Chains. *Energy* **2020**, *211*, 118701.

(15) Laroussi, M.; Bekeschus, S.; Keidar, M.; Bogaerts, A.; Fridman, A.; Lu, X.; Ostrikov, K.; Hori, M.; Stapelmann, K.; Miller, V.; Reuter, S.; Laux, C.; Mesbah, A.; Walsh, J.; Jiang, C.; Thagard, S. M.; Tanaka, H.; Liu, D.; Yan, D.; Yusupov, M. Low-Temperature Plasma for Biology, Hygiene, and Medicine: Perspective and Roadmap. *IEEE Trans. Radiat. Plasma Med. Sci.* **2022**, *6*, 127−157.

(16) Privat-Maldonado, A.; Schmidt, A.; Lin, A.; Weltmann, K.-D.; Wende, K.; Bogaerts, A.; Bekeschus, S. ROS from Physical Plasmas: Redox Chemistry for Biomedical Therapy. *Oxid. Med. Cell. Longevity* **2019**, *2019*, 9062098.

(17) Wang, H.; Zhang, X. Magnetic Fields and Reactive Oxygen Species. *Int. J. Mol. Sci.* **2017**, *18*, 2175.

(18) Filipić, A.; Gutierrez-Aguirre, I.; Primc, G.; Mozetič, M.; Dobnik, D. Cold Plasma, a New Hope in the Field of Virus Inactivation. *Trends Biotechnol.* **2020**, *38*, 1278−1291.
(19) von Woedtke, T.; Laroussi, M.; Gherardi, M. Foundations of Plasmas for Medical Applications. *Plasma Sources Sci. Technol.* **2022**, *31*, 054002.
(20) Isbary, G.; Shimizu, T.; Li, Y.-F.; Stolz, W.; Thomas, H. M.; Morfill, G. E.; Zimmermann, J. L. Cold Atmospheric Plasma Devices for Medical Issues. *Expert Rev. Med. Devices* **2013**, *10*, 367−377.
(21) Lu, X.; Laroussi, M.; Puech, V. On Atmospheric-Pressure Non-Equilibrium Plasma Jets and Plasma Bullets. *Plasma Sources Sci. Technol.* **2012**, *21*, 034005.
(22) Lin, A.; Truong, B.; Patel, S.; Kaushik, N.; Choi, E. H.; Fridman, G.; Fridman, A.; Miller, V. Nanosecond-Pulsed DBD Plasma-Generated Reactive Oxygen Species Trigger Immunogenic Cell Death in A549 Lung Carcinoma Cells through Intracellular Oxidative Stress. *Int. J. Mol. Sci.* **2017**, *18*, 966.
(23) Lin, A.; Razzokov, J.; Verswyvel, H.; Privat-Maldonado, A.; De Backer, J.; Yusupov, M.; Cardenas De La Hoz, E.; Ponsaerts, P.; Smits, E.; Bogaerts, A. Oxidation of Innate Immune Checkpoint CD47 on Cancer Cells with Non-Thermal Plasma. *Cancers* **2021**, *13*, 579.
(24) Ariën, K. K.; Heyndrickx, L.; Michiels, J.; Vereecken, K.; Van Lent, K.; Coppens, S.; Willems, B.; Pannus, P.; Martens, G. A.; Van Esbroeck, M.; Goossens, M. E.; Marchant, A.; Bartholomeeusen, K.; Desombere, I. Three Doses of BNT162b2 Vaccine Confer Neutralising Antibody Capacity against the SARS-CoV-2 Omicron Variant. *npj Vaccines* **2022**, *7*, 35.
(25) Reed, L. J.; Muench, H. A Simple Method of Estimating Fifty per Cent Endpoints. *Am. J. Epidemiol.* **1938**, *27*, 493−497.
(26) Koyama, M.; Tsujimoto, K.; Uozaki, M.; Ikeda, K.; Yamasaki, H.; Koyama, A. H.; Arakawa, T. Effects of Electrolytes on Virus Inactivation by Acidic Solutions. *Int. J. Mol. Med.* **2011**, *27*, 803−809.
(27) Oehmigen, K.; Hähnel, M.; Brandenburg, R.; Wilke, Ch.; Weltmann, K.-D.; von Woedtke, Th. The Role of Acidification for Antimicrobial Activity of Atmospheric Pressure Plasma in Liquids. *Plasma Processes Polym.* **2010**, *7*, 250−257.
(28) Lin, A.; Biscop, E.; Breen, C.; Butler, S. J.; Smits, E.; Bogaerts, A. Critical Evaluation of the Interaction of Reactive Oxygen and Nitrogen Species with Blood to Inform the Clinical Translation of Nonthermal Plasma Therapy. *Oxid. Med. Cell. Longevity* **2020**, *2020*, 9750206.
(29) Pitol, A. K.; Julian, T. R. Community Transmission of SARS-CoV-2 by Surfaces: Risks and Risk Reduction Strategies. *Environ. Sci. Technol. Lett.* **2021**, *8*, 263−269.
(30) American Type Culture Collection (ATCC). ATCC Virology Culture Guide—Converting TCID50 to Plaque Forming Units PFU. https://www.atcc.org/resources/culture-guides/virology-culture-guide (accessed Aug 8, 2022).
(31) Tarka, P.; Nitsch-Osuch, A. Evaluating the Virucidal Activity of Disinfectants According to European Union Standards. *Viruses* **2021**, *13*, 534.
(32) Keep, S.; Carr, B. V.; Lean, F. Z.; Fones, A.; Newman, J.; Dowgier, G.; Freimanis, G.; Vatzia, E.; Polo, N.; Everest, H.; Webb, I.; Mcnee, A.; Paudyal, B.; Thakur, N.; Nunez, A.; MacLoughlin, R.; Maier, H.; Hammond, J.; Bailey, D.; Waters, R.; Charleston, B.; Tuthill, T.; Britton, P.; Bickerton, E.; Tchilian, E. Porcine Respiratory Coronavirus as a Model for Acute Respiratory Coronavirus Disease. *Front. Immunol.* **2022**, *13*, 867707.
(33) Meister, S.; Verbyla, M. E.; Klinger, M.; Kohn, T. Variability in Disinfection Resistance between Currently Circulating Enterovirus B Serotypes and Strains. *Environ. Sci. Technol.* **2018**, *52*, 3696−3705.
(34) Howie, R.; Alfa, M.; Coombs, K. Survival of Enveloped and Non-Enveloped Viruses on Surfaces Compared with Other Micro-Organisms and Impact of Suboptimal Disinfectant Exposure. *J. Hosp. Infect.* **2008**, *69*, 368−376.
(35) Wang, H.; Zhao, T.; Yang, S.; Zou, L.; Wang, X.; Zhang, Y. Reactive Force Field-Based Molecular Dynamics Simulation of the Interaction between Plasma Reactive Oxygen Species and the Receptor-Binding Domain of the Spike Protein in the Capsid Protein of SARS-CoV-2. *J. Phys. D: Appl. Phys.* **2021**, *55*, 095401.
(36) Bisag, A.; Isabelli, P.; Laurita, R.; Bucci, C.; Capelli, F.; Dirani, G.; Gherardi, M.; Laghi, G.; Paglianti, A.; Sambri, V.; Colombo, V. Cold Atmospheric Plasma Inactivation of Aerosolized Microdroplets Containing Bacteria and Purified SARS-CoV-2 RNA to Contrast Airborne Indoor Transmission. *Plasma Processes Polym.* **2020**, *17*, 2000154.
(37) Bisag, A.; Isabelli, P.; Laghi, G.; Laurita, R.; Dirani, G.; Taddei, F.; Bucci, C.; Capelli, F.; Gherardi, M.; Paglianti, A.; Sambri, V.; Colombo, V. Cold Atmospheric Plasma Decontamination of SARS-CoV-2 Bioaerosols. *Plasma Processes Polym.* **2022**, *19*, No. e2100133.
(38) Moldgy, A.; Nayak, G.; Aboubakr, H. A.; Goyal, S. M.; Bruggeman, P. J. Inactivation of Virus and Bacteria Using Cold Atmospheric Pressure Air Plasmas and the Role of Reactive Nitrogen Species. *J. Phys. D: Appl. Phys.* **2020**, *53*, 434004.
(39) von Woedtke, T.; Oehmigen, K.; Brandenburg, R.; Hoder, T.; Wilke, C.; Hähnel, M.; Weltmann, K.-D. Plasma-Liquid Interactions: Chemistry and Antimicrobial Effects. *Plasma for bio-decontamination, medicine and food security*; Springer, 2012, pp 67−78.
(40) Aboubakr, H. A.; Gangal, U.; Youssef, M. M.; Goyal, S. M.; Bruggeman, P. J. Inactivation of Virus in Solution by Cold Atmospheric Pressure Plasma: Identification of Chemical Inactivation Pathways. *J. Phys. D: Appl. Phys.* **2016**, *49*, 204001.
(41) Kobza, J.; Geremek, M.; Dul, L. Ozone Concentration Levels in Urban Environments—Upper Silesia Region Case Study. *Int. J. Environ. Res. Public Health* **2021**, *18*, 1473.
(42) Wolfgruber, S.; Loibner, M.; Puff, M.; Melischnig, A.; Zatloukal, K. SARS-CoV2 Neutralizing Activity of Ozone on Porous and Non-Porous Materials. *N Biotechnol.* **2022**, *66*, 36−45.
(43) Roy, S.; Choudhury, B.; Johnson, J.; Schindler-Tyka, A. Application of Dielectric Barrier Discharge for Improving Food Shelf Life and Reducing Spoilage. *Sci. Rep.* **2021**, *11*, 1−9.
(44) Dobrynin, D.; Fridman, G.; Friedman, G.; Fridman, A. Physical and Biological Mechanisms of Direct Plasma Interaction with Living Tissue. *New J. Phys.* **2009**, *11*, 115020.
(45) Mentel, R.; Shirrmakher, R.; Kevich, A.; Dreĭzin, R.; Shmidt, I. Virus Inactivation by Hydrogen Peroxide. *Vopr. Virusol.* **1977**, *6*, 731−733.
(46) Bidra, A. S.; Pelletier, J. S.; Westover, J. B.; Frank, S.; Brown, S. M.; Tessema, B. Comparison of in Vitro Inactivation of SARS CoV-2 with Hydrogen Peroxide and Povidone-iodine Oral Antiseptic Rinses. *J. Prosthodontics* **2020**, *29*, 599−603.
(47) Mileto, D.; Mancon, A.; Staurenghi, F.; Rizzo, A.; Econdi, S.; Gismondo, M. R.; Guidotti, M. Inactivation of SARS-CoV-2 in the Liquid Phase: Are Aqueous Hydrogen Peroxide and Sodium Percarbonate Efficient Decontamination Agents? *ACS Chem. Health Saf.* **2021**, *28*, 260−267.
(48) Lin, A.; Gorbanev, Y.; De Backer, J.; Van Loenhout, J.; Van Boxem, W.; Lemière, F.; Cos, P.; Dewilde, S.; Smits, E.; Bogaerts, A. Non-Thermal Plasma as a Unique Delivery System of Short-Lived Reactive Oxygen and Nitrogen Species for Immunogenic Cell Death in Melanoma Cells. *Adv. Sci.* **2019**, *6*, 1802062.
(49) Yusupov, M.; Privat-Maldonado, A.; Cordeiro, R. M.; Verswyvel, H.; Shaw, P.; Razzokov, J.; Smits, E.; Bogaerts, A. Oxidative Damage to Hyaluronan−CD44 Interactions as an Underlying Mechanism of Action of Oxidative Stress-Inducing Cancer Therapy. *Redox Biol.* **2021**, *43*, 101968.
(50) Bogaerts, A.; Yusupov, M.; Razzokov, J.; Van der Paal, J. Plasma for Cancer Treatment: How Can RONS Penetrate through the Cell Membrane? Answers from Computer Modeling. *Front. Chem. Sci. Eng.* **2019**, *13*, 253−263.
(51) Privat-Maldonado, A.; O'Connell, D.; Welch, E.; Vann, R.; van der Woude, M. W. Spatial Dependence of DNA Damage in Bacteria Due to Low-Temperature Plasma Application as Assessed at the Single Cell Level. *Sci. Rep.* **2016**, *6*, 35646.
(52) Heilingloh, C. S.; Aufderhorst, U. W.; Schipper, L.; Dittmer, U.; Witzke, O.; Yang, D.; Zheng, X.; Sutter, K.; Trilling, M.; Alt, M.;

Steinmann, E.; Krawczyk, A. Susceptibility of SARS-CoV-2 to UV Irradiation. *Am. J. Infect. Control* **2020**, *48*, 1273−1275.
(53) Patterson, E. I.; Prince, T.; Anderson, E. R.; Casas-Sanchez, A.; Smith, S. L.; Cansado-Utrilla, C.; Solomon, T.; Griffiths, M. J.; Acosta-Serrano, Á.; Turtle, L.; Hughes, G. L. Methods of Inactivation of SARS-CoV-2 for Downstream Biological Assays. *J. Infect. Dis.* **2020**, *222*, 1462−1467.
(54) Herrmann, H. W.; Henins, I.; Park, J.; Selwyn, G. Decontamination of Chemical and Biological Warfare (CBW) Agents Using an Atmospheric Pressure Plasma Jet (APPJ). *Phys. Plasmas* **1999**, *6*, 2284−2289.
(55) Chen, Z.; Bai, F.; Jonas, S. J.; Wirz, R. E. Cold Atmospheric Plasma for Addressing the COVID-19 Pandemic. *Plasma Processes Polym.* **2022**, *19*, 2200012.
(56) Burton, J.; Love, H.; Richards, K.; Burton, C.; Summers, S.; Pitman, J.; Easterbrook, L.; Davies, K.; Spencer, P.; Killip, M.; Cane, P.; Bruce, C.; Roberts, A. D. G. The Effect of Heat-Treatment on SARS-CoV-2 Viability and Detection. *J. Virol. Methods* **2021**, *290*, 114087.
(57) Pozzetto, B.; Gaudin, O. G. COXSACKIEVIRUSES (PICORNAVIRIDAE). *Encyclopedia of Virology*; Elsevier, 1999; p 305.
(58) Chen, C. W.; Lee, H.-M.; Chang, M. B. Inactivation of Aquatic Microorganisms by Low-Frequency AC Discharges. *IEEE Trans. Plasma Sci.* **2008**, *36*, 215−219.
(59) Hänsch, M. A.; Mann, M.; Weltmann, K.-D.; von Woedtke, T. Analysis of Antibacterial Efficacy of Plasma-Treated Sodium Chloride Solutions. *J. Phys. D: Appl. Phys.* **2015**, *48*, 454001.
(60) Schmidt, M.; Hahn, V.; Altrock, B.; Gerling, T.; Gerber, I. C.; Weltmann, K.-D.; von Woedtke, T. Plasma-Activation of Larger Liquid Volumes by an Inductively-Limited Discharge for Antimicrobial Purposes. *Appl. Sci.* **2019**, *9*, 2150.
(61) Chan, K.; Sridhar, S.; Zhang, R.; Chu, H.; Fung, A.-F.; Chan, G.; Chan, J.-W.; To, K.-W.; Hung, I.-N.; Cheng, V.-C.; Yuen, K.-Y. Factors Affecting Stability and Infectivity of SARS-CoV-2. *J. Hosp. Infect.* **2020**, *106*, 226−231.
(62) Robinson, L. K. Effect of Heat and of PH on Strains of Coxsackie Virus. *Proc. Soc. Exp. Biol. Med.* **1950**, *75*, 580−582.
(63) Xie, Y.; Guo, W.; Lopez-Hernadez, A.; Teng, S.; Li, L. The PH Effects on SARS-CoV and SARS-CoV-2 Spike Proteins in the Process of Binding to HACE2. *Pathogens* **2022**, *11*, 238.
(64) Satoh, K.; MacGregor, S. J.; Anderson, J. G.; Woolsey, G. A.; Fouracre, R. A. Pulsed-Plasma Disinfection of Water Containing Escherichia Coli. *Jpn. J. Appl. Phys.* **2007**, *46*, 1137.
(65) Ikawa, S.; Kitano, K.; Hamaguchi, S. Effects of PH on Bacterial Inactivation in Aqueous Solutions Due to Low-temperature Atmospheric Pressure Plasma Application. *Plasma Processes Polym.* **2010**, *7*, 33−42.
(66) Liu, F.; Sun, P.; Bai, N.; Tian, Y.; Zhou, H.; Wei, S.; Zhou, Y.; Zhang, J.; Zhu, W.; Becker, K.; Fang, J. Inactivation of Bacteria in an Aqueous Environment by a Direct-current, Cold-atmospheric-pressure Air Plasma Microjet. *Plasma Processes Polym.* **2010**, *7*, 231−236.
(67) Kim, M.; Lawson, J.; Hervé, R.; Jakob, H.; Ganapathisubramani, B.; Keevil, C. W. Development of a Rapid Plasma Decontamination System for Decontamination and Reuse of Filtering Facepiece Respirators. *AIP Adv.* **2021**, *11*, 105311.
(68) Park, S. Y.; Ha, S.-D. Assessment of Cold Oxygen Plasma Technology for the Inactivation of Major Foodborne Viruses on Stainless Steel. *J. Food Eng.* **2018**, *223*, 42−45.
(69) Chen, Z.; Garcia, G.; Arumugaswami, V.; Wirz, R. E. Cold Atmospheric Plasma for SARS-CoV-2 Inactivation. *Phys. Fluids* **2020**, *32*, 111702.
(70) Rizan, C.; Mortimer, F.; Stancliffe, R.; Bhutta, M. F. Plastics in Healthcare: Time for a Re-Evaluation. *J. R. Soc. Med.* **2020**, *113*, 49−53.
(71) WHO. *Rational Use of Personal Protective Equipment for Coronavirus Disease (COVID-19) and Considerations during Severe Shortages: Interim Guidance*; World Health Organization, 2020.
(72) WHO. Tonnes of COVID-19 health care waste expose urgent need to improve waste management systems. https://www.who.int/news/item/01-02-2022-tonnes-of-covid-19-health-care-waste-expose-urgent-need-to-improve-waste-management-systems (accessed 2022).
(73) Zikhathile, T.; Atagana, H.; Bwapwa, J.; Sawtell, D. A Review of the Impact That Healthcare Risk Waste Treatment Technologies Have on the Environment. *Int. J. Environ. Res. Public Health* **2022**, *19*, 11967.
(74) World Health Organization. *Decontamination and Reprocessing of Medical Devices for Health-Care Facilities*, 2016.
(75) Bogaerts, A.; Neyts, E. C. Plasma Technology: An Emerging Technology for Energy Storage. *ACS Energy Lett.* **2018**, *3*, 1013−1027.
(76) Bekeschus, S.; Kramer, A.; Suffredini, E.; von Woedtke, T.; Colombo, V. Gas Plasma Technology—An Asset to Healthcare during Viral Pandemics Such as the COVID-19 Crisis? *IEEE Trans. Radiat. Plasma Med. Sci.* **2020**, *4*, 391−399.
(77) Yamashiro, R.; Misawa, T.; Sakudo, A. Key Role of Singlet Oxygen and Peroxynitrite in Viral RNA Damage during Virucidal Effect of Plasma Torch on Feline Calicivirus. *Sci. Rep.* **2018**, *8*, 17947.
(78) Nayak, G.; Aboubakr, H. A.; Goyal, S. M.; Bruggeman, P. J. Reactive Species Responsible for the Inactivation of Feline Calicivirus by a Two-dimensional Array of Integrated Coaxial Microhollow Dielectric Barrier Discharges in Air. *Plasma Processes Polym.* **2018**, *15*, 1700119.
(79) Aboubakr, H. A.; Sampedro Parra, F. S.; Collins, J.; Bruggeman, P.; Goyal, S. M. În Situ Inactivation of Human Norovirus GII. 4 by Cold Plasma: Ethidium Monoazide (EMA)-Coupled RT-QPCR Underestimates Virus Reduction and Fecal Material Suppresses Inactivation. *Food Microbiol.* **2020**, *85*, 103307.
(80) Lacombe, A.; Niemira, B. A.; Gurtler, J. B.; Sites, J.; Boyd, G.; Kingsley, D. H.; Li, X.; Chen, H. Nonthermal Inactivation of Norovirus Surrogates on Blueberries Using Atmospheric Cold Plasma. *Food Microbiol.* **2017**, *63*, 1−5.
(81) Bae, S.-C.; Park, S. Y.; Choe, W.; Ha, S.-D. Inactivation of Murine Norovirus-1 and Hepatitis A Virus on Fresh Meats by Atmospheric Pressure Plasma Jets. *Food Res. Int.* **2015**, *76*, 342−347.
(82) Obrová, K.; Vaňková, E.; Sláma, M.; Hodek, J.; Khun, J.; Ulrychová, L.; Nogueira, F.; Laos, T.; Sponseiler, I.; Kašparová, P.; Machková, A.; Weber, J.; Scholtz, V.; Lion, T. Decontamination of High-Efficiency Mask Filters From Respiratory Pathogens Including SARS-CoV-2 by Non-Thermal Plasma. *Front. Bioeng. Biotechnol.* **2022**, *10*. DOI: 10.3389/fbioe.2022.815393
(83) Cortázar, O. D.; Megía-Macías, A.; Moreno, S.; Brun, A.; Gómez-Casado, E. Vulnerability of SARS-CoV-2 and PR8 H1N1 Virus to Cold Atmospheric Plasma Activated Media. *Sci. Rep.* **2022**, *12*, 263.
(84) Guo, L.; Xu, R.; Gou, L.; Liu, Z.; Zhao, Y.; Liu, D.; Zhang, L.; Chen, H.; Kong, M. G. Mechanism of Virus Inactivation by Cold Atmospheric-Pressure Plasma and Plasma-Activated Water. *Appl. Environ. Microbiol.* **2018**, *84*, No. e007266.
(85) Gunaydin, M.; Esen, S.; Karadag, A.; Unal, N.; Yanik, K.; Odabasi, H.; Birinci, A. Vitro Antimicrobial Activity of Medilox Super-Oxidized Water. *Ann. Clin. Microbiol. Antimicrob.* **2014**, *13*, 29.